Available online at www.sciencedirect.com

ScienceDirect

Energy Procedia 63 (2014) 2448 – 2457

Energy Procedia

GHGT-12

Experiments and modelling of two-phase transient flow during pipeline depressurization of CO_2 with various N_2 compositions

Michael Drescher[a]*, Kristoffer Varholm[b], Svend T. Munkejord[b], Morten Hammer[b], Rudolf Held[a,#], Gelein de Koeijer[a]

[a]*Statoil ASA, Research, Development and Innovation, NO-7005 Trondheim, Norway*
[b]*SINTEF Energy Research, P.O. Box 4761 Sluppen, NO-7465 Trondheim, Norway*

Abstract

Pressure-release experiments of CO_2 with impurity contents of 10, 20 and 30 mol% nitrogen have been executed. The experimental investigations were performed in a 140 m long horizontal tube with an inner diameter of 10 mm. The initial conditions of the CO_2-N_2 mixtures were in the supercritical region at approximately 120 bar and 20 °C. The results, which showed a good repeatability, were then compared with numerical data from a homogeneous equilibrium model. The investigations have concentrated on the pressure wave at the start as well as the pressure and temperature development during the pressure release. The model, which has a certain complexity, but still contains several simplifications, gave relatively good results for all three gas mixtures. Although the absolute values for the temperature development showed to be consistently higher in the experimental results compared to the numerical results, the liquid dry-out points were predicted with good accuracy at all measurement points. The numerical results of the pressure development match the experimental results very well, both regarding the absolute and relative values. Regarding the speed of the pressure wave, the numerical results were consistently too high, which is believed to be caused by the EOS overpredicting the speed of sound for our cases. The good results, especially for the pressure, are promising, and further work is suggested to improve the model.

Peer-review under responsibility of the Organizing Committee of GHGT-12

Keywords: CO_2 transport; Depressurization; Pressure wave; Impurities; Experiments; Model

* Corresponding author. Tel.: +47 97003339
E-mail address: midr@statoil.com

[#] New affiliation: Wintershall Holding GmbH, Kassel, Germany

Peer-review under responsibility of the Organizing Committee of GHGT-12
doi:10.1016/j.egypro.2014.11.267

1. Introduction

Detailed knowledge on depressurization of CO_2 pipelines has shown to be important for safe and cost-effective design of CO_2 Capture & Storage (CCS) chains. CO_2 is normally transported by pipeline in a liquid, dense or vapour-liquid phase at high pressure. Depressurizations can occur during planned operations, maintenance or undesirable accidents. The most extreme case is a pipeline rupture due to e.g. pipeline corrosion or external force, during which a crack will form accompanied by a sudden depressurization of CO_2. If the internal pipeline pressure at the tip of the crack is above a certain threshold, the fracture will propagate. Simultaneously, the depressurization leads to the start of a pressure-relief front or pressure wave in the pipeline. In theory, the fracture might propagate indefinitely if the fracture-propagation speed is faster than the pressure wave of the fluid caused by the rupture [1].

One way of preventing such a running fracture is by installing mechanical crack arrestors. However, the preferred way is by dimensioning the pipeline with a minimum required toughness which assures shorter fracture lengths [2]. Therefore, detailed knowledge of the pressure wave is needed for safe and cost-efficient design of the pipeline. However, CO_2 from sources such as natural gas processing or flue gas of fossil-fuel power plants typically contain impurities to a certain extent, which in turn alter the fluid properties. This will have to be accounted for by flow models for CO_2 transport [3,4]. Furthermore, such models must be able to handle two-phase flow, both for depressurization and normal operation [5].

Fracture propagation control involves a coupled fluid-structure problem. In order to provide improved predictions for CO_2 mixtures and high-toughness steel types, coupled fluid-structure models are under development [6–11]. To develop and verify flow models for the depressurization of CO_2-rich mixtures, there is a need for experimental data. Although data exist for natural gas [12], little has been published for CO_2. In this work, therefore, pressure-release experiments have been executed with various amounts of nitrogen as impurity. To illuminate the observed phenomena, the data from experimental investigations are then compared with numerical data from solving a homogeneous equilibrium model (HEM). The paper will present and discuss the measured and simulated results, focusing on the pressure wave picked up at the start of the depressurization as well as on the pressure and temperature development.

2. Test Facility

For executing the experimental investigations the horizontal flow circuit of the CO_2 transport test facility at Statoil's R&D center in Trondheim, Norway was used. The horizontal flow circuit consists of a 140 m long horizontal stainless steel tube with an inner diameter of 10 mm and a wall thickness of 1 mm as shown in Figure 1. The steel has a density of 8000 kg/m^3, a specific heat capacity of 485 J/(kg K) and a thermal conductivity of 14 W/(m K). Further information is found in Pettersen et al. [13] and De Koeijer et al. [14].

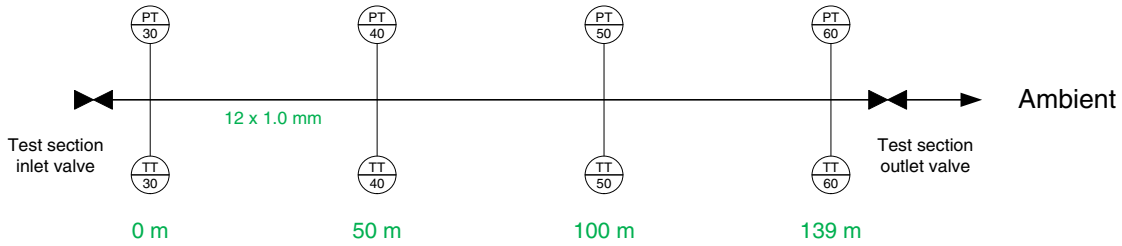

Figure 1: Set-up of the horizontal flow circuit.

The horizontal flow circuit is filled at the inlet valve at 0 m. At 140 m the outlet valve is situated which will be operated during the pressure release. The outlet valve is a near full bore ball valve with an inner diameter of 9.5 mm, which is slightly less than the horizontal flow tube. The horizontal flow circuit is located inside a container and coiled up under the roof. During pressure-release investigations a 1.9 m long straight horizontal tube with the same

dimensions as the horizontal flow circuit is connected downstream to the outlet valve, which guides the mixture to a safe location.

The circuit is instrumented with temperature and pressure sensors at approximately 0 m, 50 m, 100 m and 139 m, as seen in Figure 1. A more detailed description of the respective positions is given in Table 1.

Table 1: Positions of valves and instruments in the test section.

Position	Description
0.0 m	Test section inlet valve
0.2 m	Pressure sensor 1 (PT-30)
0.7 m	Temperature element 1 (TT-30)
50.7 m	Pressure sensor 2 (PT-40)
51.2 m	Temperature element 2 (TT-40)
101.2 m	Pressure sensor 3 (PT-50)
101.7 m	Temperature element 3 (TT-50)
139.2 m	Pressure sensor 4 (PT-60)
139.7 m	Temperature element 4 (TT-60)
140.0 m	Test section outlet valve
141.9 m	Ambient

The temperature development during the investigations were measured by four thermocouples of type T. Each had a diameter of 3.2 mm and was placed slightly inside the stream of the mixture. The sensors had an estimated uncertainty of ±1 K. For measuring the pressure, and in particular the initial pressure wave, four UNIK 5000 high frequency response pressure transmitters from GE were installed. They had a frequency response of 5 kHz and an accuracy of ±0.13 bar. For logging the high frequency data a National Instruments PXI system was used which logged the temperature with 80 Hz. The pressure was logged with a speed of 5 kHz for the first 10 seconds to capture the pressure wave. Thereafter, the pressure was logged with 100 Hz.

3. Experimental Investigations

For investigating the speed of the pressure wave of CO_2 with impurities, pressure release investigations with different contents of nitrogen as impurity were executed. The impurity content was varied between 10, 20 and 30 mol%. As initial conditions for the mixtures, a pressure of 120 bar and a temperature of approximately 20 °C was chosen. The reason was to ensure start-up from the supercritical region and to use the same initial test conditions for the varying mixtures, hence avoiding the two-phase area to prevent possible condensation and therewith separation of the two components. The test matrix with the measured initial conditions is shown in Table 2. Each pressure release was repeated at least once to confirm repeatability. In the following we plot results from the first experiment (#1) unless otherwise stated.

Table 2: Test matrix of the pressure release investigations.

N_2 [mol%]	#	Pressure [bar]	Temperature [°C]	Ambient temp. [°C]
10.2	1	119.9	19.5	18.4
	2	119.9	19.1	18.1
20.0	1	120.8	19.7	19.5
	2	119.9	17.9	18.1
30.0	1	120.0	17.3	17.4
	2	120.0	20.4	18.9
	3	119.9	16.1	15.1

To ensure the respective gas-mixture compositions, premixed gas mixtures in gas bottles from a gas vendor were used. The relative inaccuracy amounted to 2 % of the certified mixture. To achieve the desired test pressure, the gas was then compressed using on oil free gas booster. The temperature of the mixture was controlled by adjusting the ambient temperature inside the test container. After the pressure and temperature have equalized inside the test section, the high-speed logging was started quickly followed by manually opening the test-section outlet valve.

4. Models

4.1. Flow model and thermophysical properties

The flow in the tube is modelled as one-dimensional single- or two-phase flow where there is a strong coupling between the gas and the liquid, such that they travel at a common velocity. In addition, full equilibrium in pressure, temperature and chemical potential is assumed. This is described by the homogeneous equilibrium model (HEM):

$$\frac{\partial \rho}{\partial t} + \frac{\partial}{\partial x}(\rho u) = 0 \qquad \text{(Conservation of mass)} \tag{1}$$

$$\frac{\partial}{\partial t}(\rho u) + \frac{\partial}{\partial x}(\rho u^2 + p) = -F_w \qquad \text{(Momentum balance)} \tag{2}$$

$$\frac{\partial E}{\partial t} + \frac{\partial}{\partial x}[u(E+p)] = Q \qquad \text{(Energy balance)} \tag{3}$$

where $\rho = \rho_g \alpha_g + \rho_l \alpha_l$ and $E = \rho\,(e + \tfrac{1}{2}\,u^2)$ are the mixture density and total energy, respectively. Herein, α is the volume fraction and e is the specific internal energy. F_w is the wall friction and Q is the heat-transfer rate through the tube wall. Subscripts g and l denote the gas and liquid phase. The flow equations are advanced in time using a multi-stage (MUSTA) finite-volume scheme [15,16] on a uniform grid. Different grids and CFL numbers have been considered to evaluate the sensitivity. As a result, a grid of 1000 cells and a CFL number of 0.85 have been employed in the present work.

The Peng–Robinson [17] equation of state was used. Classical Van der Waals mixing rules were applied to account for the multicomponent fluid in the problem at hand. The TRAPP method [18,19] was used to compute the dynamic viscosity and thermal conductivity of the fluid. The state-function-based approach of Michelsen [20] is used to calculate pressure, temperature and phase distribution given mixture density, specific internal energy and composition.

4.2. Friction model

The wall friction is calculated as

$$Fw = \begin{cases} f_j \dfrac{\dot{m}|\dot{m}|}{2\rho_j d_i} & \text{Single phase } (j = g, l) \\ f_l \dfrac{\dot{m}|\dot{m}|}{2\rho_l d_i}\Phi & \text{Two-phase (Friedel)} \end{cases} \tag{4}$$

Here $f_j = f\,(Re_j)$ is the Darcy friction factor, $Re_j = \dot{m}\, d_i/\mu_j$ is the Reynolds number for phase j and $\dot{m} = \rho u$ is the mass-flux density. The coefficient Φ is an empirical correlation, which is used to account for two-phase flow, and depends on various properties of both phases. Here we have employed the Friedel [21] correlation. The details of the calculation of the two-phase coefficient Φ, and also further discussion, can be found in Aakenes [22,23].

4.3. Heat transfer

The steel tube has a non-negligible heat capacity which needs to be taken into account. This is done by solving the heat equation

$$\rho c_p \frac{\partial T}{\partial t} - \frac{1}{r}\frac{\partial}{\partial r}\left(\lambda r \frac{\partial T}{\partial r}\right) = 0 \tag{5}$$

along with the flow model, assuming radial symmetry and that axial conduction can be neglected. Herein, ρ, c_p and λ are the density, specific heat capacity and thermal conductivity, respectively, of the steel. For solving (5), ten radial cells are employed.

For the inner heat-transfer coefficient, h_i , we use the Nusselt-number correlation:

$$Nu = \begin{cases} 3.66 & Re < 2300 \\ 0.023 Re^{4/5} Pr^{1/3} & Re > 3000 \quad \text{(Colburn)} \end{cases} \tag{6}$$

with linear interpolation in the region 2300 < *Re* < 3000. See e.g. Bejan [24], Chap. 6. Here *Pr* is the Prandtl number:

$$Nu = \frac{h_i d_i}{\lambda_f}, \quad \mathrm{Pr} = \frac{c_{f,p}\mu_f}{\lambda_f} \tag{7}$$

where subscript *f* indicates fluid properties. The outer heat-transfer coefficient is assumed to be constant, h_o = 20 W/(m^2 K).

4.4. Outlet boundary conditions

Our numerical model does currently not cater for valves inside the tube. We therefore approximate the setup in Figure 1 by simulating a tube of length 141.9 m with a valve at the end. The valve is a manually operated ball valve, which is modelled by specifying the outlet pressure as follows:

$$p(t) = \begin{cases} p_0 + (p_i - p_0)\cos\left(\dfrac{\pi t}{2t_\delta}\right) & 0 \le t < t_\delta \\ p_0 & t \ge t_\delta \end{cases} \tag{8}$$

Herein, p_i is the initial tube pressure and p_0 is the ambient pressure. The time to open the valve is estimated to be t_δ = 0.1 s. Due to the hyperbolic nature of the flow equations, the outlet pressure of the tube will not be the ambient pressure, but rather a choke pressure, during much of the simulation.

5. Results & Discussion

Figure 2–Figure 5 show model predictions and experimental data for the four positions indicated in Figure 1. In the figures, 70%, 80% and 90% indicate the CO_2 contents, cf. Table 2. For the temperature (left-hand column) it can be seen that the temperature drops faster for 70% CO_2, particularly at the closed end of the tube (Figure 2), but 90% CO_2 attains the lowest temperature. At the outlet (Figure 5), the coldest measured temperature is about –35°C for 90% CO_2, versus about –15°C for 70% CO_2. Regarding the pressure (right-hand column) we observe that the pressure drops fastest in the beginning for 90% CO_2, but after about 5s, the lowest pressure is measured for 70% CO_2. One reason for this is that for 90% CO_2, the process stays longer at a supercritical pressure before entering into

the two-phase region, at which point the mixture speed of sound drops significantly. This effect is most pronounced near the closed end of the tube (Figure 2 and Figure 3).

In general, there is good agreement between experiments and calculations for the pressure (right-hand column). For the temperature (left-hand column), the correspondence between calculations and experiments is quite good in the middle of the tube (Figure 3 and Figure 4), but the calculated temperature is in general lower than the measured one. The minima in the calculated temperature profiles correspond to dry-out, i.e., the point in time where the last liquid is evaporated. In Figures 3, 4 and 5, i.e. for the middle and open end of the tube, it can be seen that calculated and measured time for dry-out agree well, for all the CO_2-mixture compositions. It can also be observed that dry-out happens first near the outlet, which is expected. In Figure 2, for the closed end of the tube, it appears that dry-out happens somewhat later than predicted by the model for 80 and 90% CO_2.

For the closed end of the tube (Figure 2), the calculated temperatures are significantly lower than the measured ones. In particular, this is true at dry-out. We assume that a reason for this may be that the Colburn heat-transfer correlation does not sufficiently account for the effect of boiling. The inherent assumption in the homogeneous equilibrium model of no slip may also not hold very well at the closed end of the tube, where the velocities are small. In the present case, it may also be that the temperature sensors have some delay due to their relatively large size.

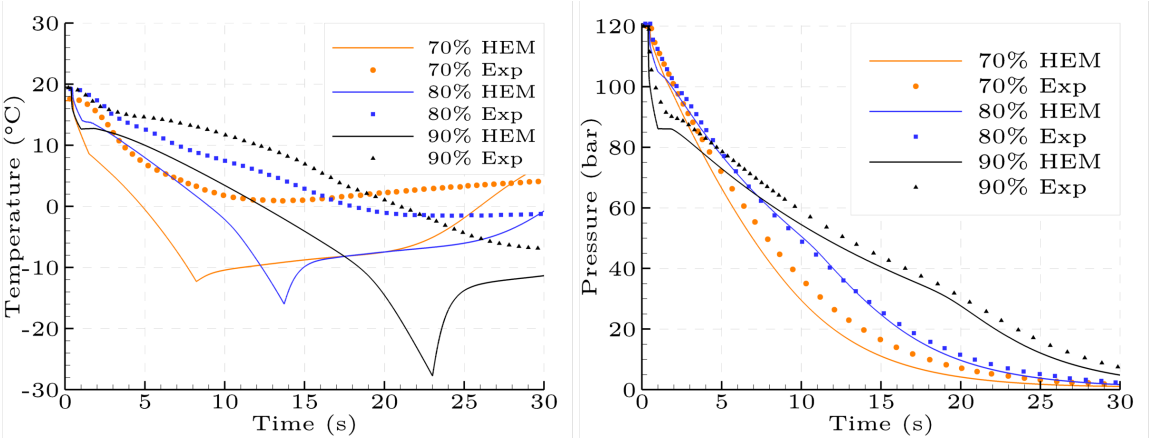

Figure 2: Comparison of experimental data (PT-30, TT-30) and numerical solutions for different compositions at 0 m (closed end of the tube).

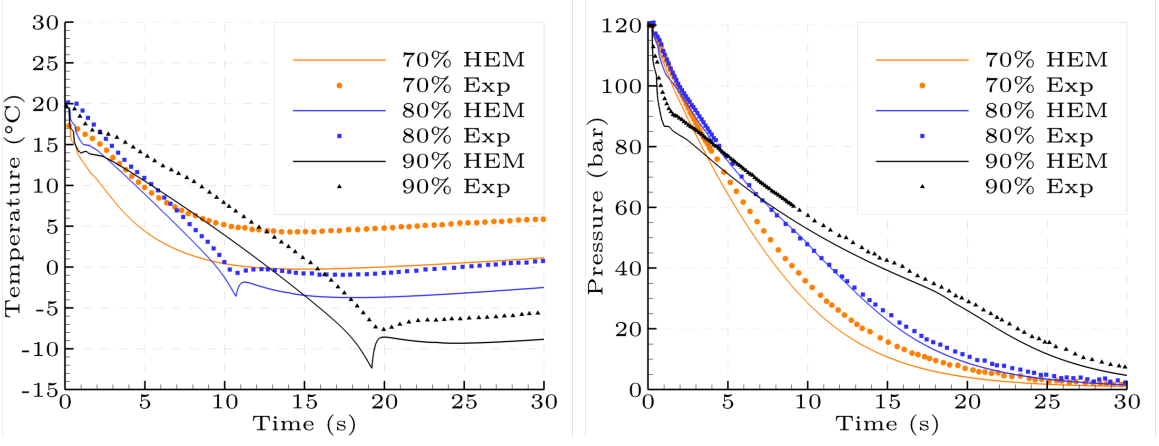

Figure 3: Comparison of experimental data (PT-40, TT-40) and numerical solutions for different compositions at 50 m.

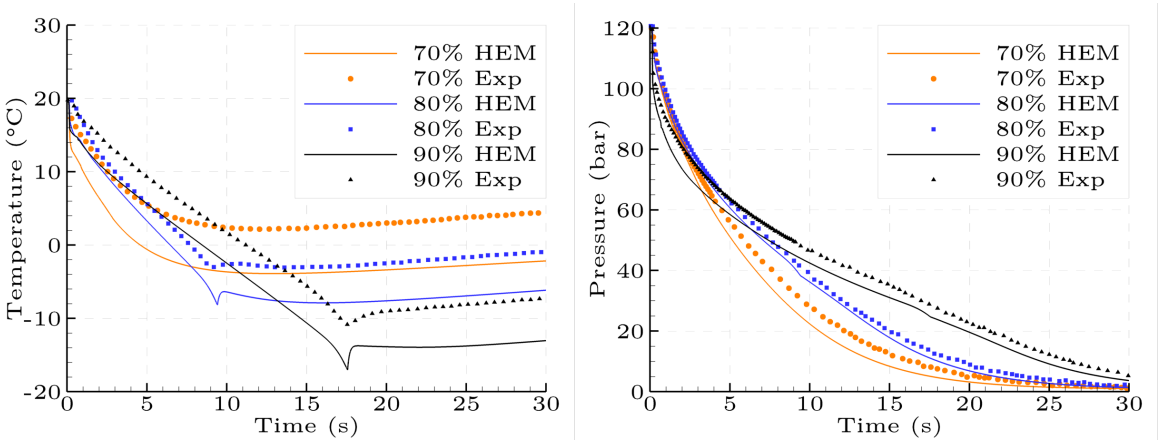

Figure 4: Comparison of experimental data (PT-50, TT-50) and numerical solutions for different compositions at 100 m.

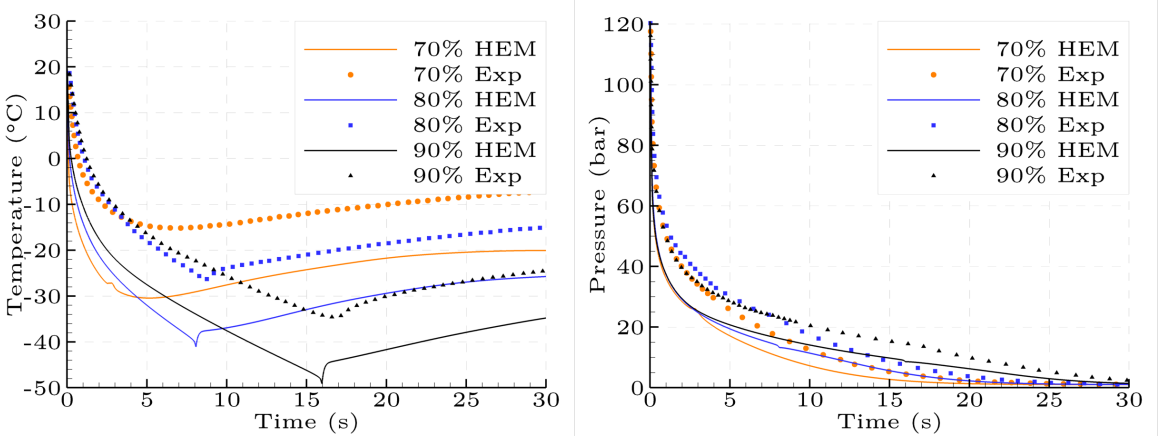

Figure 5: Comparison of experimental data (PT-60, TT-60) and numerical solutions for different compositions at 139 m (open end of the tube).

The calculated and measured time to dry-out at the open end of the tube for 10 and 20 % N_2 are given in Table 3. It can be seen that the agreement is good; the model predicts dry-out slightly before this is indicated by the temperature measurements, between 5.4% and 10.2% earlier. Since the numerical model but also the experimental data for a nitrogen composition of 30 % do not show a distinct dry-out point, this composition was omitted.

Table 3: Time to dry-out at open end of tube.

N_2 [mol%]	**#**	**Experimental [s]**	**Numerical [s]**	**Num–Exp [s]**
10.2	1	16.88	15.97	–0.91 (–5.4%)
	2	18.01	16.17	–1.84 (–10.2%)
20.0	1	8.62	8.07	–0.55 (–6.4%)
	2	–	–	–

Figure 6 shows the pressure drop recorded during the first 0.8 seconds of the experimental investigations for 10% N_2. The time for the pressure wave to travel from PT-60 to PT-30 amounted to 414 ms for the first test and 403 ms for the second test. Similar plots can be made for the other tests with the compositions of 20 and 30% N_2. Further, corresponding data can be extracted from the calculations. Since the fluid is initially at rest, the results can be compared and give an indication of how well the model predicts the speed of sound. The results are shown in Table 4. It can be seen that the experimental data are consistent, which shows a good repeatability. Furthermore, the numerical data show that the pressure-propagation speed is overpredicted by the model, from around 10% for 10% N_2 to approximately 23% for 20% N_2. The overprediction is most likely due to the use of the Peng–Robinson EOS.

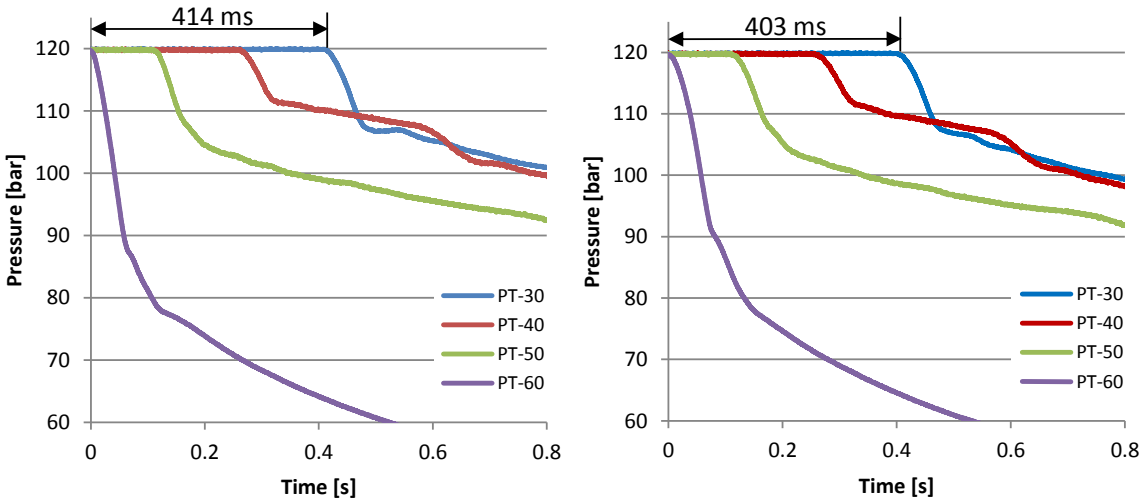

Figure 6: Pressure wave recorded for the tests with 10 mol% N_2 (#1 to the left and #2 to the right) as a function of time at given locations.

Table 4: Travel times for the initial pressure wave from PT-60 to PT-30.

N_2 [mol%]	#	Experimental [ms]	Numerical [ms]	Num–Exp [ms]
10.2	1	414	368	–46 (–11.1%)
	2	403	366	–37 (–9.2%)
20.0	1	565	443	–122 (–21.6%)
	2	572	443	–129 (–22.6%)
30.0	1	561	467	–94 (–16.7%)
	2	555	467	–88 (–15.9%)
	3	561	465	–96 (–17.1%)

Calculated pressure profiles at 0.1 s intervals are shown in Figure 7. It illustrates the initial pressure wave (rarefaction wave) which travels across the length of the tube, and which is reflected at the closed end. The wave amplitude diminishes mainly due to wall friction. The figure shows that the pressure drops rapidly at first and then levels off. This is an attribute of the drop in speed of sound when coming from the single phase region to the two-phase region.

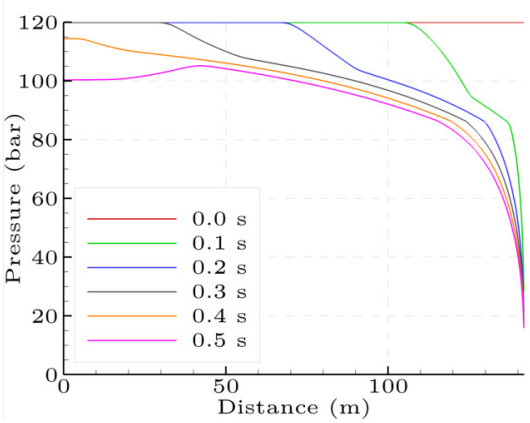

Figure 7: Calculated pressure profiles at 0.1 s intervals for test run #1 with 10 mol% N_2.

6. Conclusions

Pressure-release investigations have been performed in a tube filled with CO_2 and 10%, 20% and 30% N_2. High-frequency pressure sensors were employed and good repeatability was obtained. We observe that the temperature drops faster and dry-out occurs earlier for higher nitrogen content. However, the coldest temperature occurs for 10% N_2. The pressure initially drops faster for lower nitrogen content, particularly near the closed end of the tube. After approximately 5 s, the pressure is higher for low nitrogen content, meaning that the tube is emptied slower.

The data from the experimental investigations have been compared to calculations from a homogeneous equilibrium model. The absolute values for the temperature development during the pressure release showed to be consistently higher in the experimental results compared to the numerical results. This is believed to be the result of two main effects; the use of a simple heat-transfer correlation inside the tube which may underpredict the heat transfer due to boiling, as well as the rather large size of the temperature sensors which results in a somewhat slow response. Still, quite good results were achieved for the temperatures measured in the middle of the test section. However, the discrepancies between the experimental and numerical data for the measurement points at the ends were significantly larger for all three fluid compositions. Further, the dry-out points were predicted with good accuracy at all measurement points. Here it should be noted that at the closed end of the tube, dry-out occurred gradually without any distinct points.

The numerical results for the pressure development during the pressure release match the experimental results very well, both regarding the absolute and relative values. This is true both for the different positions along the tube and for all three fluid compositions.

Regarding the speed of the pressure-wave which was picked up by the high-response pressure transmitters in the experimental investigations, the numerical results were consistently too high. This is mainly due to the Peng-Robinson EOS overpredicting the speed of sound for our cases.

The employed homogeneous equilibrium model including transient heat transfer to the surroundings has a certain complexity, but still contains several simplifications. In view of this, the relatively good results, particularly for the pressure, are encouraging. Further work could include more advanced heat-transfer models taking into account the effect of boiling or flow regimes. In addition, further experimental investigations could be executed using improved temperature sensors which are more sensitive to the occurring temperature drop during pressure release. This will probably reduce the absolute discrepancies observed between the numerical and experimental results.

Acknowledgements

The modelling work was performed in the CO_2 Dynamics project. The authors acknowledge the support from the Research Council of Norway (189978), Gassco AS, Statoil Petroleum AS and Vattenfall AB. The experimental data were provided by Statoil from the CO_2 IT IS project funded by the Research Council of Norway (188940) and Statoil.

References

[1] Oosterkamp, A. and Ramsen J., State-of-the-Art Overview of CO_2 Pipeline Transport with relevance to offshore pipelines, Polytec Report number: POL-O-2007-138-A, 2008

[2] Cosham A., Eiber R.J., Fracture Control in Carbon Dioxide Pipelines: The Effect of Impurities, 7th International Pipeline Conference, Vol. 3, Calgary, Alberta, Canada, 2008

[3] Munkejord S.T., Jakobsen J.P., Austegard A. and Mølnvik M.J. Thermo- and fluid-dynamical modelling of two-phase multi-component carbon dioxide mixtures. *Int. J. Greenh. Gas Con*. 2010;4:589–596.

[4] Aursand, P., Hammer, M., Munkejord, S. T. and Wilhelmsen, Ø. Pipeline transport of CO_2 mixtures: Models for transient simulation. Int. J. Greenh. Gas Con. 2013; 15:174-185.

[5] Munkejord S.T., Bernstone C., Clausen S., de Koeijer G., Mølnvik M.J. Combining thermodynamic and fluid flow modelling for CO_2 flow assurance. *Energy Procedia* 2013;37:2904-13

[6] Berstad, T., Dørum, C., Jakobsen, J.P., Kragset, S., Li, H., Lund, H., Morin, A., Munkejord, S.T., Mølnvik, M.J., Nordhagen, H.O. and Østby, E. CO_2 pipeline integrity: A new evaluation methodology, *Energy Procedia* 2011;4,:3000–3007.

[7] Nordhagen, H.O., Kragset, S., Berstad, T., Morin, A., Dørum, C. and Munkejord, S.T. A new coupled fluid-structure modelling methodology for running ductile fracture. *Comput. Struct*. 2012;94–95:1006–1014.

[8] Aursand, E., Aursand P., Berstad, T., Dørum, C., Hammer, M., Munkejord, S. T. and Nordhagen, H. O. CO_2 pipeline integrity: A coupled fluid-structure model using a reference equation of state for CO_2. *Energy Procedia* 2013; 37:3113-3122.

[9] Aursand, E., Dørum, C., Hammer, M., Morin, A., Munkejord, S. T. and Nordhagen, H. O. CO_2 pipeline integrity: Comparison of a coupled fluid-structure model and uncoupled two-curve methods. *Energy Procedia* 2014; 51C: 382-391.

[10] Mahgerefteh, H., Brown, S. and Denton, G. Modelling the impact of stream impurities on ductile fractures in CO_2 pipelines. *Chem. Eng. Sci.* 2012;74:200–210.

[11] Aihara S, Misawa K. Numerical simulation of unstable crack propagation and arrest in CO_2 pipelines. First International Forum on the Transportation of CO_2 by Pipeline; Gateshead, UK. 2010.

[12] Botros, K.K., Geerligs, J., Rothwell, B., Carlson, L., Fletcher, L., Venton, P. Measurements of flow parameters and decompression wave speed following rupture of rich gas pipelines, and comparison with GASDECOM. *Int. J. Pres. Ves. Pip.* 2010; 87:681–695.

[13] Pettersen J., de Koeijer G., Hafner A., Construction of a CO_2 pipeline test rig for R&D and operator training, GHGT-8, Norway

[14] de Koeijer G., Borch J.H., Jakobsen J., Hafner A., Experiments and modelling of CO_2 pipeline depressurization – Multi-phase transient flow, The 4th Trondheim Conference on CO_2 Capture, Transport and Storage, Trondheim, Norway, 2007

[15] Toro, E.F., and Titarev, V.A. MUSTA fluxes for systems of conservation laws, *J. Comput. Phys.* 2006; 216, pp. 403–429.

[16] Munkejord S.T., Evje S. and Flåtten T. The multi-stage centred-scheme approach applied to a drift-flux two-phase flow model. *Int. J. Numer. Meth. Fluids* 2006; 52:679–705.

[17] Peng, R.Y. and Robinson, D.B. A new two-constant equation of state. *Ind. Eng. Chem. Fund.* 1976; 15:59–64.

[18] Ely, J.F. and Hanley, H.J.M. Prediction of transport properties. 1. Viscosity of fluids and mixtures. *Ind. Eng. Chem. Fund.* 1981; 20:323–332.

[19] Ely, J.F. and Hanley, H.J.M. Prediction of transport properties. 2. Thermal conductivity of pure fluids and mixtures. *Ind. Eng. Chem. Fund.* 1983; 22:90–97.

[20] Michelsen, M.L. State function based flash specifications. *Fluid Phase Equilib*. 1999; 158-160:617-626.

[21] Friedel, L. Improved friction pressure drop correlations for horizontal and vertical two phase pipe flow, in: Proceedings, European Two Phase Flow Group Meeting, Ispra, Italy, 1979, paper E2.

[22] Aakenes, F. Frictional pressure-drop models for steady-state and transient two-phase flow of carbon dioxide, Master's thesis, Department of Energy and Process Engineering, Norwegian University of Science and Technology (NTNU), 2012.

[23] Aakenes, F., Munkejord, S.T. and Drescher, M. Frictional pressure drop for two-phase flow of carbon dioxide in a tube: Comparison between models and experimental data. *Energy Procedia* 2014; 51C:373–381.

[24] Bejan, A. *Heat Transfer*. Wiley, New York, 1993.